JOURNAL OF MATERIALS SCIENCE 20 (1985) 3683–3690

Ti_nO_{2n-1} Magnéli phase formation in $SrTiO_3$ dielectrics

MASAYUKI FUJIMOTO*, MAMORU WATANABE‡
Department of Materials Science and Engineering, Massachusetts Institute of Technology, Cambridge, Massachusetts 02139, USA

Electron diffraction, high-resolution transmission electron microscopy and scanning transmission electron microscopy reveal that Ti_nO_{2n-1} Magnéli phases, Ti_4O_7, Ti_5O_9 and others, exist at the multiple grain junctions in strontium titanate dielectrics. A new type of ledge structure detected at coherent grain boundaries in the Ti_4O_7 phase is characterized in detail. The $SrTiO_3$ grain and the second phase maintains a particular orientation relationship. Epitaxial growth of Ti_4O_7 from the silica-rich liquid phase occurs during cooling; the crystal growth geometry of Ti_4O_7 is related to the directly observed atomically rough interface and atomically smooth interface.

1. Introduction

There is an homologous series of oxides with the formula Ti_nO_{2n-1}, the so-called "Magnéli phase", between Ti_2O_3 (corundum type) and TiO_2 (rutile). Studies have been made of the crystal structures of the Ti_nO_{2n-1} family over the last two decades. X-ray powder diffraction studies first revealed the existence of a homologous series of oxides with the formula Ti_nO_{2n-1} ($4 \leqslant n \leqslant 10$) [1]. Among them the structure of Ti_5O_9 was analysed by single crystal X-ray diffraction technique [2]. The ideal Ti_5O_9 structure can be described as being derived from the idealized rutile by first removing every tenth oxygen-only-plane parallel to $(1\,2\,1)_r$[§] and then displacing the adjacent rutile slabs by approximately $(1/2)\ [0\,1\,1]_r$. The slabs are of infinite extension in two dimensions and have a characteristic finite width corresponding to n, the number of TiO_6 octahedra linked in the third direction. The end octahedra of a slab share faces with those of the neighbouring slabs, the atomic arrangement in the corundum type structure. The metal atom positions in the titanium lattice are anti-phase, while the oxygen lattice is continuous, which is the reason for terming them "crystallographic shear" (CS) structures. The CS operation $(1/2)\langle 0\,1\,1\rangle_r\{1\,2\,1\}_r$ is regularly recurrent [3]. This model was successfully used to interpret the X-ray powder patterns of the other members in the series [4].

Electron microscopy and diffraction techniques established the existence of ordered CS structures, Ti_nO_{2n-1} ($16 \leqslant n \leqslant 36$), with the same displacement vector acting across the $(1\,3\,2)_r$ plane. The CS plane rotates continuously from $(1\,3\,2)_r$ to $(1\,2\,1)_r$, about a $(1\,1\,1)_r$ zone axis, producing a continuous series of high-index intermediate CS planes with $(h\,k\,l)_r = p(1\,2\,1)_r + q(0\,1\,1)_r$ where p and q are integers [5–7].

The CS structure is formed by MO_6 octahedra sharing oxygen atoms with neighbours. Since this face-sharing necessarily results in metal ions coming close to each other, the potential distribution in the crystal becomes periodically steep on the basis of CS planes forming a new wider super cell. Consequently the CS region ought to be darker in contrast in transmission electron microscopy (TEM) high resolution image taken under optimum defocusing, sufficient resolution

Permanent address: Taiyo Yuden Co Ltd, 1660 Kamisatomi, Haruna-machi, Gunma-gun, Gunma 370-33, Japan.
‡ *Present address*: National Institute for Research in Inorganic Materials, 1-1 Namiki, Sakura-mura, Niihari-gun, Ibaraki 305, Japan.
§ The subscript r denotes rutile indices.

0022–2461/85 $03.00 + .12

limit and so on. This is one of the reasons why defect structure studies using the high-resolution TEM technique have concentrated on materials having the CS structure.

Among recent studies of TiO_2 Magnéli phase CS structure using high resolution transmission electron microscopy, a point-to-point resolution of 0.16 nm on the image of Ti_6O_{11} was shown using top entry style JEOL 100 CX equipped with ultra-high resolution pole pieces (where the spherical aberration constant C_s = 0.7 mm) [8]. However, computer-simulation techniques indicate that the useful information about defect structures can be obtained even with 0.3 nm resolution, when the project charge density approximation can be applied for sufficiently thin crystals [9]. The (1 1 0) CS structure has been studied using a JEOL 200 CX with a high resolution goniometer stage (C_s = 1.1 mm) [10], while a study of the CS structure by means of a high voltage transmission electron microscope has also been performed [11]. Mechanisms of reduction and oxidation, twinning and coherent boundary structures in evaporated Ti_4O_7 thin films were studied in the interpretable resolution range using 1 MeV TEM; coherent twin boundaries having (1 0 4)Ti_4O_7 = $\{0\,1\,1\}_r$ twinning plane, coherent intergrowth of Ti_5O_9 and Ti_6O_{11} parallel to (0 0 2) of Ti_4O_7 and possibly a new metastable Ti_5O_9 (1 3 2) CS structure that forms coherent boundaries parallel to $(1\,0\,2)_r$ = (2 3 5) of Ti_4O_7 [11].

In this paper, the existence of Ti_nO_{2n-1} Magnéli phases in $SrTiO_3$ dielectrics is revealed by electron diffraction, high-resolution TEM images and scanning transmission electron microscopy (STEM) chemical analysis. The formation of Magnéli phases and the coherent boundary structures observed in Ti_4O_7 are discussed from a crystallographical point of view.

2. Experimental method

A non-stoichiometric mixture of $SrCO_3$[¶] (1.000 mol) and TiO_2* (1.004 mol) with Nb_2O_5 (0.002 mol) and small amounts of SiO_2 and Al_2O_3 (0.004 wt % and 0.002 wt %, respectively) of chemical reagent grade 99% purity were prepared by wet milling for 20 h. The mixture was calcined at 1000° C for 2 h in air. The formation of $SrTiO_3$ was confirmed by X-ray powder diffraction. The product was pressed into discs 15 mm diameter and 3 mm thick at a pressure of 1000 kg cm^{-2}. The pressed discs were sintered at 1450° C for 3 h in a reducing atmosphere (nitrogen 95% + hydrogen 5%) and cooled to room temperature in the furnace under the reducing atmosphere.

Sintered specimens were mechanically ground to less than 0.1 mm in thickness using a diamond disc. One of them was re-fired in a specially designed rapid quenching furnace for 1 h at 1450° C and rapidly quenched into water from 1450° C [12]. The calculated quenching rate is about 1.6 × 10^4 ° C sec^{-1}. The quenched sample and the furnace-cooled one were further thinned by ion micromilling with argon ions accelerated through a potential of 5 kV and 0.5 mA until perforation was observed. The thinned specimens were observed by TEM JEOL 200 CX extensive use side entry style with high resolution pole pieces (C_s = 1.9 mm and C_c = 1.9 mm, where C_c is the chromatic aberration constant). For the measurement of reciprocal spacing in electron diffraction a gold film was evaporated on the supporting film and was used as an internal standard. The chemical composition in the same areas was analysed by STEM VG HB-5 equipped with a Kevex detector for energy dispersive X-ray analysis. The probe diameter and current in the STEM were approximately 2.5 nm and 10^{-8} A, respectively, under an accelerating voltage of 100 kV. The specimen was held in a graphite-nosed cartridge which allowed translation and tilting but which did not contribute spurious X-rays to the signal. As the STEM electron microprobe caused severe damage to specimens, STEM chemical analysis was always carried out after TEM observation.

3. Results and interpretation

3.1. Multiple grain junctions

3.1.1. Slowly cooled samples

The TEM images and electron diffraction patterns of multiple grain junctions in slowly cooled samples are complicated due to the coexistence of several kinds of second phases (crystalline phases and an amorphous phase) and to microtwinning of the crystalline phases. X-ray energy spectra from the amorphous phase shows high silica composition. Some of the crystal second

[¶]Kanto Chemical Co.
*Toho Titan Co.

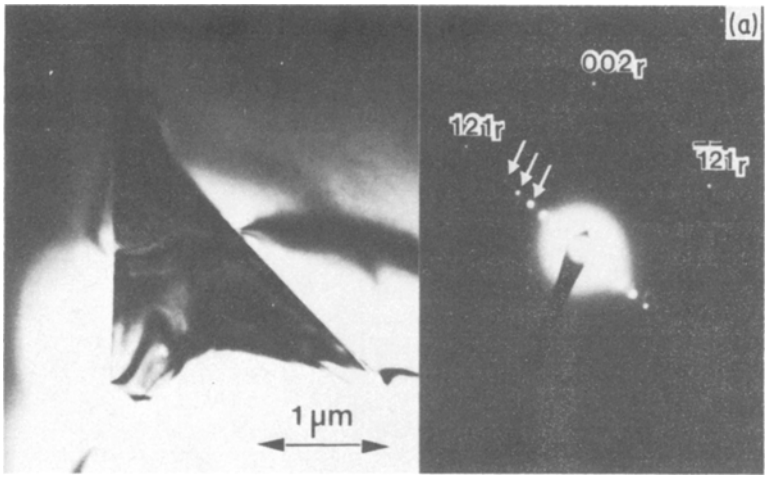

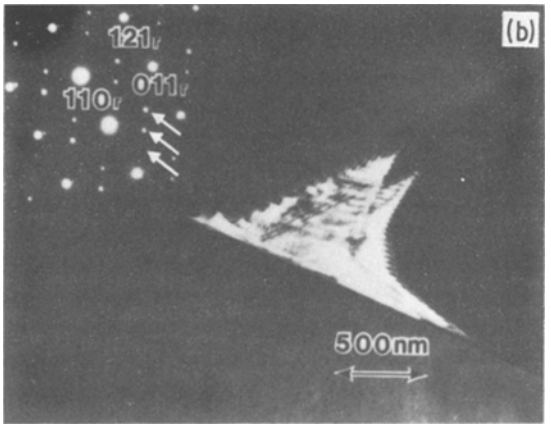

Figure 1 (a) Bright-field image of Ti_9O_{17} second phase at the grain junction. The eight additional spots between 0 0 0 and 1 2 1 reflections are indicated by the arrows in the diffraction pattern. The strong reflections are derived from rutile subcell structure. (b) Dark-field image of Ti_5O_9 second phase at the grain junction. The four satellites between 0 0 0 and 1 2 1 reflections are indicated by the arrows in the diffraction pattern.

phases show satellites in addition to the rutile-type lattice diffraction spots; their STEM spectra give only one strong characteristic X-ray peak, Ti$K\alpha$ [13].

Considering these results and the reducing atmosphere in the sintering and cooling process, the formation of Magnéli phases may be expected. In fact, an electron diffraction pattern shown in Fig. 1a as an example can be well indexed on the basis of the lattice of Ti_9O_{17}. Another example in Fig. 1b can be interpreted as Ti_5O_9. Usually, several kinds of Magnéli phases with different "n" were found in a given specimen; Ti_4O_7 to Ti_9O_{17}. According to the diffraction patterns, those phases contain the CS planes on the $(1\,2\,1)_r$. The number of satellites between 0 0 0 and 1 2 1 reflections is related to the number n in the formula of Ti_nO_{2n-1}.

3.1.2. Rapidly quenched samples

No diffraction spots were detected from multiple grain junctions in specimens rapidly quenched. Accordingly, putting the smallest objective aperture on an halo in a diffraction pattern, the TEM-dark field image in Fig. 2b was taken, which shows clearly bright contrast of the glassy material as compared with $SrTiO_3$, and the junction is completely filled with it. This situation was observed for most junctions in quenched samples. The STEM energy dispersive X-ray spectrum indicates that the amorphous material is rich in silicon with strontium, titanium (Ti > Sr) and small amounts of aluminium, magnesium, iron and copper (iron and copper probably from the stainless steel holder of ion mill and copper micro grid, respectively, during the ion thinning process).

3.2. Microstructure at multiple grain junctions in slowly cooled samples

3.2.1. Band structure and coherent boundary

The lattice image in Fig. 3a and STEM spectrum were obtained from a specimen consisting of the second phase partially etched out and the adjacent $SrTiO_3$ grain. The electron diffraction pattern in Fig. 4 was taken including both of them. The reflection spots from the grain can be recognized by moving a selected area diffraction

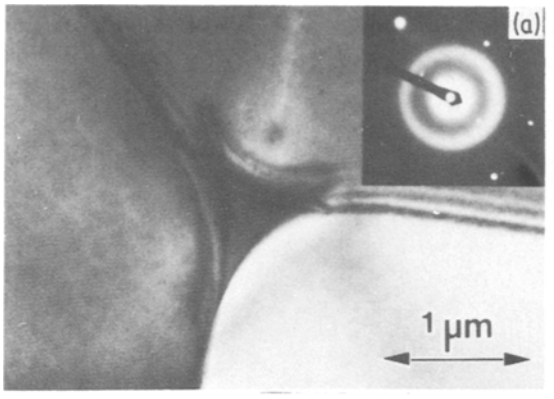

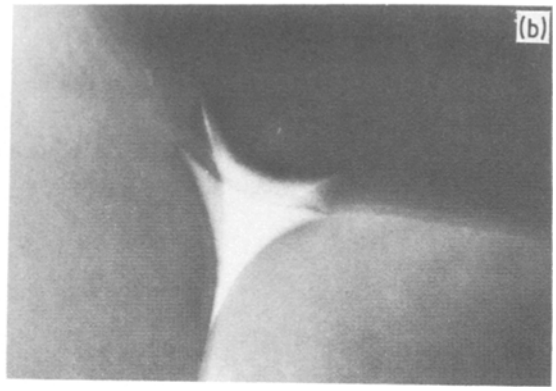

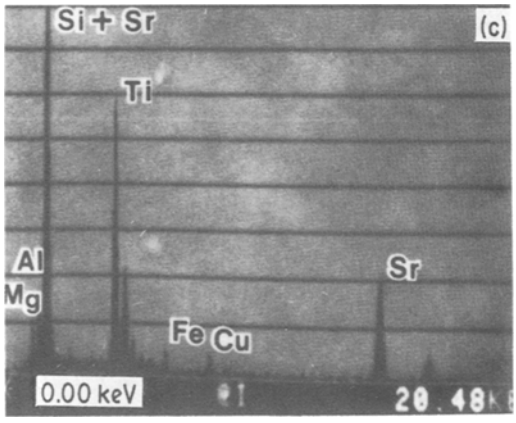

Figure 2 (a) Bright-field image of the triple grain junction in a rapidly quenched sample. The amorphous halo is observed in the diffraction pattern. (b) Dark-field image of the triple grain junction. For image formation the smallest objective aperture was put on the amorphous halo in the diffraction pattern. (c) STEM X-ray energy spectrum from the amorphous phase. Sr$K\alpha$ and Si$L\alpha$ peaks are overlapping. The strontium concentration was estimated using the Sr$L\alpha$ peak (right side of spectrum). The spectrum shows Si > Ti > Sr and small amounts of Al and Mg.

aperature. The spacings which are regarded to be from the second phase are in good agreement with those of Ti_4O_7. Indexing was made on the basis of the Ti_4O_7 triclinic unit cell having a = 0.5593 nm, b = 0.7125 nm, c = 1.2456 nm, α = 95.2°, β = 95.21° and γ O = 108.73° [4]. The diffraction pattern is composite between two reciprocal lattices with different orientations, which are coherent as described below. Both lattices ($\mathbf{a}_1^*$, $\mathbf{c}_1^*$) and ($\mathbf{a}_2^*$, $\mathbf{c}_2^*$) are twinned sharing the b-axis and rotating about 95° around the axis with each other. Furthermore, the (2 0 0) $SrTiO_3$ diffraction spot and $\mathbf{a}_2^*$ and $\mathbf{c}_1^*$ vectors of Ti_4O_7 are on the same line in the diffraction pattern. It can be noticed that there is diffraction streak along the line at the (2 0 0) $SrTiO_3$ reciprocal spot. This is due to the lattice misfit between $SrTiO_3$ and Ti_4O_7 or lattice distortion of the $SrTiO_3$ grain at the interface. A secondary feature the periodic modulation shown in the inset (Fig. 4). It shows another structural modulation to be placed along the [1 0 8] direction. The direction and spacing of the satellite spots in the enlarged inset of Fig. 4 correspond to the band structure direction and averaged band width observed in the TEM image (indicated by the arrows in Fig. 3a) correspond to the band structure direction and averaged band width (about 5 to 10 nm) observed in the TEM image. Fig. 5a is a high-resolution image corresponding to the band structure image in Fig. 3a. This micrograph was taken from a part near the edge of the specimen under the same diffraction condition with that in Fig. 3a. Arrays of closely spaced and differently oriented white dots can be seen in each band. These form two lattices whose interplanar spacings correspond to the 1 0 0 and 0 0 2 diffraction spots observed in Fig. 4. Fig. 5b illustrates the coherent grain boundary structure observed in Fig. 5a. Ti_4O_7 (1 0 0) and (0 0 1) planes are considered to form a periodic ledge structure for the relaxation of repulsion among closely spaced titanium atoms. The steaks indicated in the enlarged inset of Fig. 4 may result from a band width distribution and lattice spacing difference between (1 0 0)Ti_4O_7 and (0 0 1)Ti_4O_7.

This type of coherent boundary has not been previously reported for Ti_4O_7.

3.2.2. Crystal growth geometry

Fig. 6a shows the grown crystallites on a "flat" grain at the multiple grain junction. Crystallites

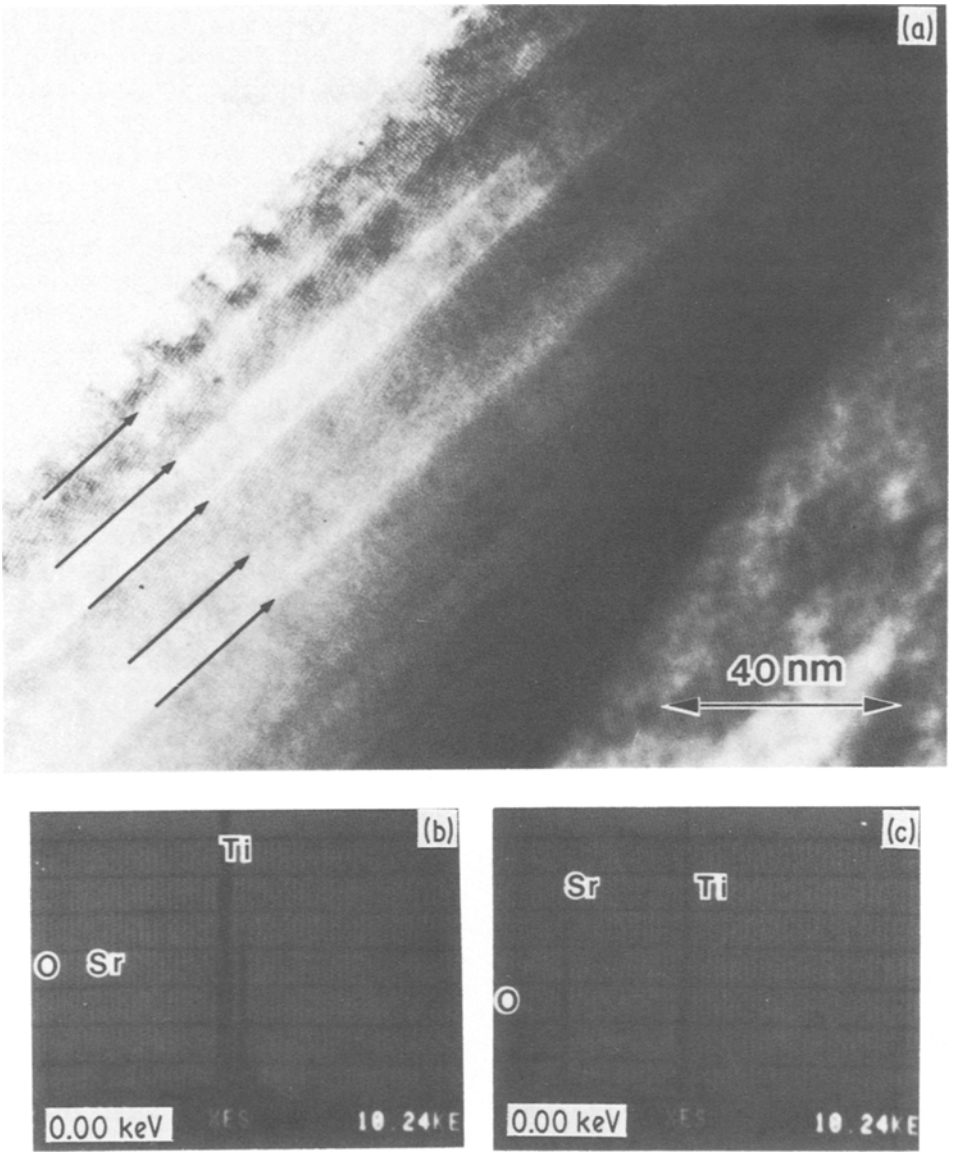

Figure 3 (a) Lattice image of second phase with "flat" grain. The specimen was partially etched out during the ion milling process for TEM specimen preparation. The band structure is indicated by the arrows. (b) X-ray energy spectrum from the second phase partially etched out. There is only the strong Ti$K\alpha$ peak. (c) X-ray energy spectrum from the "flat" grain. Ti$K\alpha$ and Sr$K\alpha$ peaks of similar intensity are observed.

and flat grain are Ti_4O_7 and $SrTiO_3$ respectively; the diffraction pattern shown in Fig. 6b which is obtained from both is the same as Fig. 4. It also shows the same crystallographical relationship between $SrTiO_3$ grain and Ti_4O_7 as in the Fig. 4; that is, the (2 0 0)$SrTiO_3$ diffraction spot and Ti_4O_7 $\mathbf{a}_2^*$ and $\mathbf{c}_1^*$ vectors are on the same line.

The enlarged images, Figs. 6c and d, show the two kinds of atomic order interface between the grown Ti_4O_7 crystallite and the amorphous phase. One is a rough interface at the narrow edge and the other is a smooth interface at the wide edge. The amorphous phase chemical composition was checked using STEM. Fig. 6e shows the X-ray energy spectrum from the amorphous phase. There is no longer a Ti$K\alpha$ peak such as was observed in the quenched amorphous phase.

The crystallites have been partially etched out during ion milling process for TEM sample

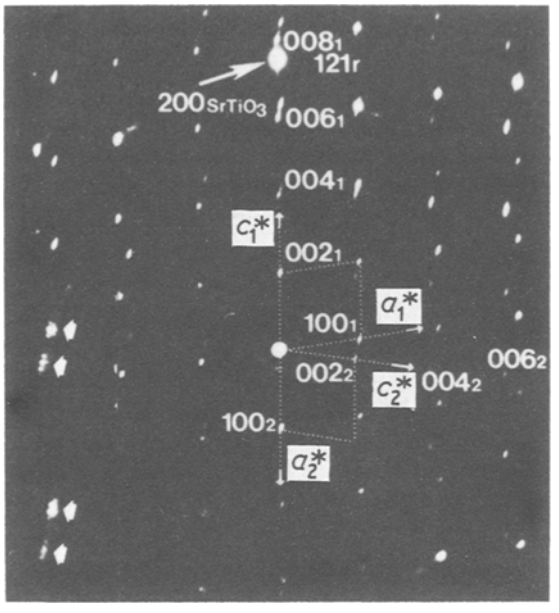

Figure 4 Electron diffraction obtained from the second phase and the grain. Indexing was made on the basis of the Ti_4O_7 triclinic unit cell having $a = 0.5593$ nm, $b = 0.7125$ nm, $c = 1.2456$ nm, $\alpha = 95.2°$, $\beta = 95.21°$ and $\gamma = 108.73°$. Two lattices, ($\mathbf{a}_1^*$, $\mathbf{c}_1^*$) and ($\mathbf{a}_2^*$, $\mathbf{c}_2^*$) are twinned sharing the b-axis and rotated about 95° around the axis of each other. Each diffraction spot is elongated along [1 0 8] to consist of several satellites as shown in the enlarged inset.

preparation; however, octagon-shaped crystal growth geometry can be recognized as indicated in Fig. 6f.

4. Discussion

Generally, in slowly cooled samples, Magnéli phases and a high silica amorphous phase (including very small amount of strontium and aluminium) coexist at grain junctions, while there is only a Si > Ti > Sr and Al glassy phase at the junctions in rapidly quenched samples. Obviously, this composition difference between the two amorphous phases is due to the formation of Magnéli phases during the cooling process after sintering. The detected ions from the latter amorphous phase, silicon, titanium and strontium, are known as network-former, intermediate and modifier in the structure of glass. Cations with a limited capability to substitute for silica in the glass network and with a strong oxygen bond strength cannot be accommodated in large concentrations in the glass. Therefore, excess titanium ions form Ti_nO_{2n-1} Magnéli phases on $SrTiO_3$ grains during cooling.

The particular Ti_4O_7 crystallite shape shown in Fig. 6a indicates the geometry of crystal growth from the liquid phase. There is a crystal growth velocity difference between two structural different planes, one with a smooth atomic interface plane and the other with a rough atomic interface plane (Figs. 6c and d). The thermodynamic driving force for solidification can be described as follows [14],

$$\Delta G = (\pi\sigma g V_s)/a.$$

where V_s is the molar volume, σ is surface energy, g is the diffuseness parameter and a is the interplanar spacing. For a flat interface, g is of the order of one, while for a rough interface g can be much smaller.

If a crystal grows with an atomically rough surface, the mobility of the interface is isotropic. The liquid atoms attach themselves freely and independently on any surface orientation that presents itself; that is, the holes or pockets in the rough surface are available for the

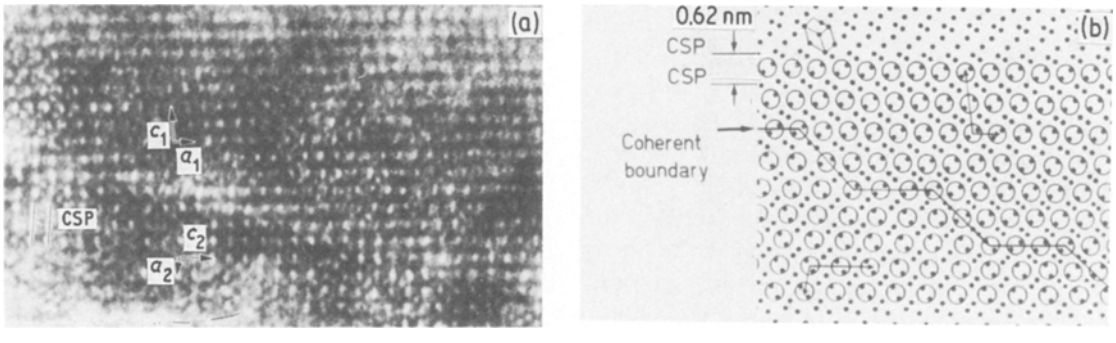

Figure 5 (a) High-resolution image corresponding to the band structure image shown in Fig. 3a. CS plane and Ti_4O_7 unit cells are indicated. (b) Schematic illustration of coherent grain-boundary structure shown in (a). Small black spots represent the position of titanium atoms. Open circles indicate the white dots observed in (a). A rutile unit cell is also shown.

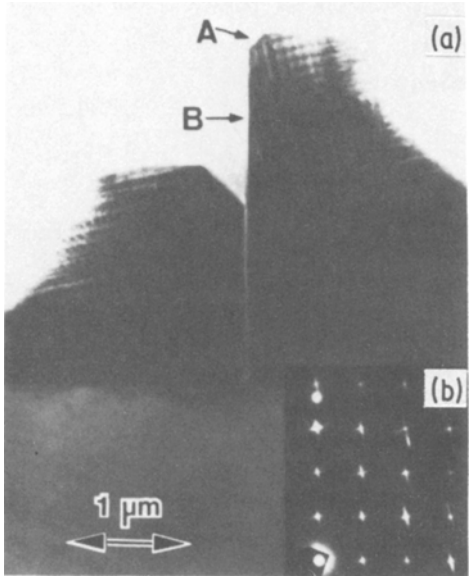

Figure 6 (a) Bright-field image of grown crystallites on a "flat" grain. The crystallites were partially etched out. (b) Electron diffraction from the crystallites and grain. (c) High-resolution image of atomically rough interface between crystallite and amorphous phase indicated by arrow A in (a). (d) High-resolution image of atomically smooth interface between crystallite and amorphous phase indicated by arrow B in (a). (e) STEM X-ray spectrum from amorphous phase. There is only the strong Si$L\alpha$ peak. (f) Expected geometry of crystallites shown in (a).

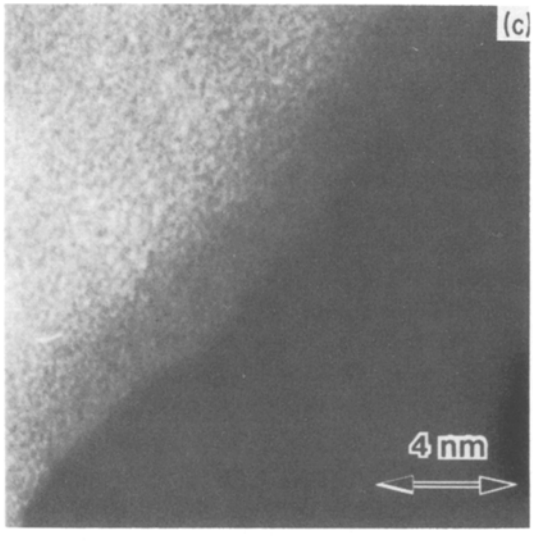

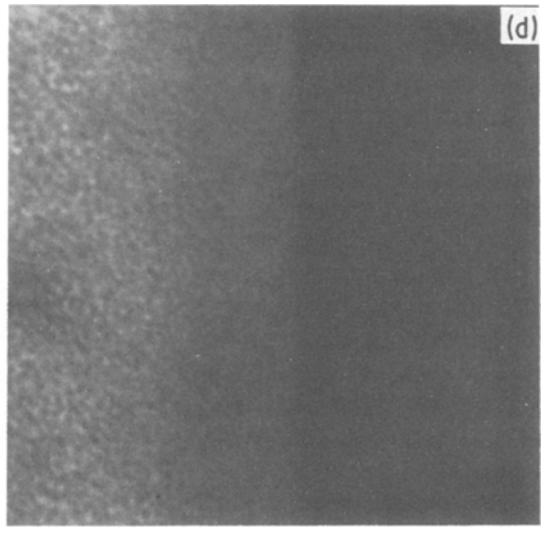

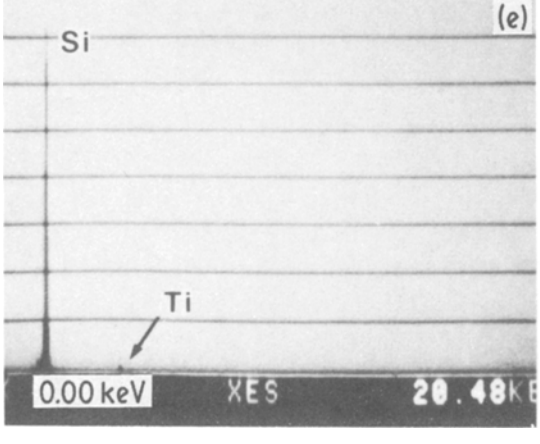

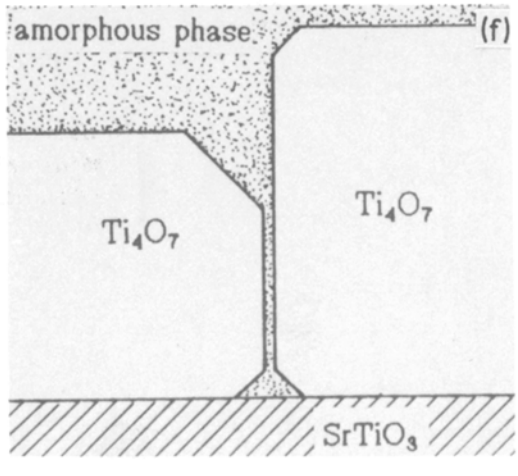

accommodation of a liquid atom as it joins the crystal. If a crystal grows with an atomically smooth surface, liquid atoms are added only at steps and the crystallinity of the surface is more apparent. In this case the existing steps will grow easily, but the formation of a new step on a surface presents a two-dimensional nucleation problem. Any small cluster of such atoms is only loosely attached to the crystal and the atoms in the cluster may melt again before they form a supercritical cluster.

Therefore, the rough surface can grow faster than the flat surface. In other words, a less closely packed plane has a faster velocity as compared with closed packed plane. Results from the geometry of Ti_4O_7 crystal growth from a silicon-rich liquid phase indicate that (1 0 0) and (0 0 1) planes are the closed packed planes in Ti_4O_7.

Some of electron diffraction patterns show obvious orientation relationships between them (Figs. 4 and 6b). The (2 0 0)$SrTiO_3$ diffraction spot, Ti_4O_7 $\mathbf{a}_2^*$ and $\mathbf{c}_1^*$ vectors are on the same line in the diffraction pattern. The Ti_4O_7(0 0 1) and (1 0 0) planes in the coherent structure are parallel to the $SrTiO_3$(1 0 0) plane. In the structure of strontium titanate, TiO_6 octahedrons occupy the corners of the cubic unit cell. The rutile structure consists of rectilinear ribbons of edge-shaped TiO_6 octahedra which are joined by corner sharing with adjacent ribbons; the orientations of adjacent ribbons differ by 90°, and the unit cell is tetragonal. This rutile structure remains a sub-cell in the Ti_4O_7 CS structure. There is a structural resemblance between TiO_2 rutile and $SrTiO_3$. Both are made of a three-dimensional TiO_6 octahedron frame work. Ti_4O_7 epitaxial growth occurs on the $SrTiO_3$ grain from the silica-rich amorphous phase: $SrTiO_3$(1 0 0)$\|$ Ti_4O_7(1 0 0) and (0 0 1).

The direction of the observed coherent boundaries is Ti_4O_7[1 0 8], which has a special orientation relationship with the $SrTiO_3$(1 0 0) plane. While the precise interface structure remains unclear, the lattice parameters of the $SrTiO_3$(1 0 0) and the Ti_4O_7(1 0 0) and (0 0 1) planes differ. The epitaxial growth may be responsible for the development of the coherent grain boundaries and resulting band structure.

Acknowledgement

The authors are grateful to Yet-Ming Chiang and A. J. Garratt-Reed for carrying out STEM chemical analysis and to Dunbar Birnie III for quenching a sample from the sintering temperature. Also the authors are grateful to Professor W. David Kingery for his encouragement and useful discussions. This research was supported by the Department of Energy under Contract No. DE-ACO2-76ERO2390.

References

1. S. ANDERSSON, B. COLLÉN, U. KURENTERUNA and A. MAGNÉLI, *Acta Chem. Scand.* **11** (1957) 1641.
2. S. ANDERSSON, *ibid.* **14** (1960) 1161.
3. S. ANDERSSON and L. JAHNBERG, *Arkiv fur Kemi* **11** (1963) 413.
4. J. S. ANDERSON and B. G. HYDE, *J. Phys. Chem. Solid* **28** (1967) 1393.
5. L. A. BURSILL, B. G. HYDE, O. TERASAKI and D. WATANABE, *Phil. Mag.* **20** (1969) 347.
6. L. A. BURSILL and B. G. HYDE, *Proc. R. Soc.* **A320** (1970) 147.
7. *Idem. Acta Crystallogr.* **B27** (1971) 210.
8. L. A. BURSILL and G. J. WOOD, *Phil. Mag.* **A38** (1978) 637.
9. D. F. LYNCH, A. F. MOODIE and M. A. O'KEEF, *Acta Crystallogr.* **A31** (1975) 300.
10. T. MIYANO, M. IWATANI, H. HARADA, C. KAITO and M. SHIOJIRI, *Phil. Mag.* **A48** (1983) 163.
11. K. YOSHIDA, Y. YAMADA, H. OTA, L. A. BURSILL and G. J. WOOD, *ibid.* **A44** (1981) 73.
12. D. P. BIRNIE III and W. D. KINGERY, *J. Mater. Sci.* **20** (1985) 2193.
13. M. FUJIMOTO and W. D. KINGERY, *J. Amer. Ceram. Soc.* **68** (1985) 169.
14. J. W. CAHN, *Acta Metall.* **8** (1960) 554.

Received 22 October
and accepted 22 November 1984